Journal of Power Sources 196 (2011) 3503–3512

Contents lists available at ScienceDirect

Journal of Power Sources

journal homepage: www.elsevier.com/locate/jpowsour

Kinetic analysis of carbon monoxide and methanol oxidation on high performance carbon-supported Pt–Ru electrocatalyst for direct methanol fuel cells

Amado Velázquez-Palenzuela, Francesc Centellas, José Antonio Garrido, Conchita Arias, Rosa María Rodríguez, Enric Brillas, Pere-Lluís Cabot*

Laboratori d'Electroquímica dels Materials i del Medi Ambient, Departament de Química Física, Universitat de Barcelona, Martí i Franquès 1-11, 08028 Barcelona, Spain

ARTICLE INFO

Article history:
Received 8 November 2010
Accepted 11 December 2010
Available online 21 December 2010

Keywords:
Pt–Ru nanoparticles
Electrocatalysis
Methanol oxidation reaction
Temkin isotherm
Kinetic parameters

ABSTRACT

The kinetic parameters of carbon monoxide and methanol oxidation reactions on a high performance carbon-supported Pt–Ru electrocatalyst (HP 20% 1:1 Pt–Ru alloy on Vulcan XC-72 carbon black) have been studied using cyclic voltammetry and rotating disk electrode (RDE) techniques in 0.50 M H_2SO_4 and H_2SO_4 (0.06–0.92 M) + CH_3OH (0.10–1.00 M) solutions at 25.0–45.0 °C. CO oxidation showed an irreversible behaviour with an adsorption control giving an exchange current density of 2.3×10^{-6} A cm^{-2} and a Tafel slope of 113 mV dec^{-1} ($\alpha = 0.52$) at 25.0 °C. Methanol oxidation behaved as an irreversible mixed-controlled reaction, probably with generation of a soluble intermediate (such as HCHO or HCOOH), showing an exchange current density of 7.4×10^{-6} A cm^{-2} and a Tafel slope of 199 mV dec^{-1} ($\alpha = 0.30$) at 25.0 °C. Reaction orders of 0.5 for methanol and −0.5 for proton were found, which are compatible with the consideration of the reaction between Pt–CO and Ru–OH species as the rate-determining step, being the initial methanol adsorption adjustable to a Temkin isotherm. The activation energy calculated through Arrhenius plots was 58 kJ mol^{-1}, practically independent of the applied potential. Methanol oxidation on carbon-supported Pt–Ru electrocatalyst was improved by multiple potential cycles, indicating the generation of hydrous ruthenium oxide, RuO_xH_y, which enhances the process.

1. Introduction

Direct methanol fuel cells (DMFCs) are electrical power devices based on the methanol electro-oxidation in the anode from reaction (1) [1]:

$$CH_3OH + H_2O \rightarrow CO_2 + 6H^+ + 6e^- \quad (1)$$

DMFCs have been considered as convenient power sources because of their advantages such as high energy density and efficiency, low weight, applications to portable systems, fast recharge-time and use of an easy-handling liquid fuel. However, important obstacles must be still solved in order to enable the viability of the DMFCs commercialization, highlighting the relatively poor kinetics of the methanol oxidation on the anode, generally Pt-based, in front of hydrogen oxidation, which presents a much lower overpotential [2]. Additional relevant problems are related to the generation of carbon monoxide and other species with general structure CH_xO that remain strongly adsorbed, poisoning the active sites for the methanol oxidation. The performance of DMFCs is also affected by the methanol crossover to the cathode by diffusion through the proton exchange membrane, causing a mixed potential that reduces the fuel cell efficiency.

To deal with the above problems, several papers [3–34] have reported the development of new CO-tolerant electrocatalysts for the methanol oxidation, based principally on carbon-supported (black carbon, nanofibers, mesoporous carbon, etc.) Pt–Ru electrocatalysts (Pt–Ru/C), although other binary and ternary alloys, with generally poorer results, have also been tested [6,8,15,18,19,22,33]. Most of these electrocatalysts have been synthesized by mild-temperature impregnation methods [23] using the corresponding precursor salts for the generation of the metallic nanoparticles. However, more refined alternatives have been proposed. For example, Shao et al. [27] prepared Pt–Ru nanoparticles by potentiostatic electrodeposition on Ti mesh, whereas Guo et al. [13] synthesized hollow Pt–Ru nanospheres on multi-walled carbon nanofibers and Alayoglu et al. [3] prepared Ru–Pt core–shell unsupported nanoparticles. In the case of the Pt–Ru/C electrocatalyst, the bimetallic system allows achieving a higher tolerance in front of the CO/CH_xO poisoning because of the generation of adsorbed hydroxyl species on the oxophilic Ru atoms by the electrochemical discharge of

* Corresponding author. Tel.: +34 93 4039236; fax: +34 93 4021231.
E-mail address: p.cabot@ub.edu (P.-L. Cabot).

0378-7753/$ – see front matter © 2010 Elsevier B.V. All rights reserved.
doi:10.1016/j.jpowsour.2010.12.044

water, according to reaction (2) [30]:

$$Ru + H_2O \rightarrow Ru\text{–}OH + H^+ + e^- \quad (2)$$

Afterwards, the CO molecules or the CH_xO adsorbed-intermediates poisoning neighbour Pt atoms are oxidized by interaction with the Ru-hydroxylated species, following the so-called bifunctional mechanism described by reaction (3) [30]:

$$Pt\text{–}CO + Ru\text{–}OH \rightarrow Pt + Ru + CO_2 + H^+ + e^- \quad (3)$$

The promotion effect of the Pt–Ru alloy in the modification of the electronic structure of Pt by the introduction of Ru atoms, leading to the weakening of the Pt–CO bond, has also been proposed [3]. Taking into account that the methanol oxidation leads to the production of CO as intermediate product, it is supposed that the electrocatalyst performance for both species must be related. In fact, the reaction between the Pt–CO and the Ru–OH is considered the rate-determining step in the methanol oxidation, although the methanol dissociative adsorption has been also proposed [9,25]. According to the bifunctional mechanism, a Pt–Ru 1:1 ratio is expected to be the most suitable combination to obtain the maximum DMFC performance, allowing the interaction between the neighbour metallic atoms. However, different Pt–Ru atomic ratios have been proposed. Thus, Arico et al. [4] reported the most favourable alloy composition containing 50% of Ru by comparison of fuel cell tests at 130 °C, decreasing drastically with higher Ru fractions. In contrast, Gasteiger et al. [9] found a lower optimum composition of only 10% of Ru. Alternatively, Iwasita et al. [14] described a similar performance for Ru-modified Pt (1 1 1) electrodes in the composition range of 10–40%. Other works reported intermediate atomic compositions of 25% [21], 31% [17] and 38% [26] of Ru. The disparity of these results can be related to the different Pt–Ru atomic stoichiometry on the nanoparticle surface, which is the true electrocatalyst interface and it is not necessarily coincident with the bulk composition. In fact, Liu et al. [20], using X-ray absorption spectroscopy (XAS) analysis, showed that Pt–Ru nanoparticles usually present a quite stable core–shell structure with a Ru-enriched surface due to the more favoured diffusion of Ru atoms to the outer layer during nanoparticle synthesis. Despite this, the 1:1 stoichiometry is still considered as the reference composition for Pt–Ru/C electrocatalysts.

On the other hand, adsorbed intermediates such as CO or CH_xO species have been detected during the methanol oxidation on Pt-based electrocatalysts by infrared spectroscopy (IR) [32] or differential electrochemical mass spectrometry (DEMS) [25]. Besides, using high performance liquid chromatography (HPLC) [5], formaldehyde (HCHO) and formic acid (HCOOH) were also identified as main intermediates, which can be generated from the incomplete methanol oxidation following reactions (4) and (5), respectively:

$$CH_3OH \rightarrow HCHO + 2H^+ + 2e^- \quad (4)$$

$$HCHO + H_2O \rightarrow HCOOH + 2H^+ + 2e^- \quad (5)$$

The detection of these species suggests that an alternative mechanism route involving soluble intermediates is possible, leading to a double-pathway reaction. Fig. 1 shows plausible reaction sequences from the above experimental evidences. Consequently, the methanol oxidation reaction in a fuel cell configuration can be strongly affected by mass-transport conditions in case of weak adsorption, because of the removal of the soluble intermediates from the vicinity of the electrocatalyst surface on account of the continuous reagent effluent flow, originating a decrease of the fuel cell efficiency. Hydrodynamic techniques like rotating disk electrode (RDE) can then be used to clarify the oxidation mechanism and it has been employed for analyzing the methanol kinetics of carbon-supported Pt nanoparticles [10].

In the present work cyclic voltammetry and RDE measurements are used to analyse the methanol oxidation mechanism on the selected high performance Pt–Ru/C model electrocatalyst. Complementary experiments with different potential scan rate, methanol concentration, pH and temperature are carried out in order to validate the methanol oxidation reaction pathway. In addition, CO stripping voltammetries are previously evaluated to understand the nature of the alcohol oxidation on the alloy system through the comparison of the kinetics of both reactions. Moreover, the temperature effect on the Tafel plots for the methanol oxidation is subject of special interest in our work, setting a new topic that has not been previously reported in the literature.

2. Experimental

2.1. Materials and reagents

High performance (HP) 20% 1:1 Pt–Ru alloy on Vulcan XC-72 carbon black (Pt– Ru/C electrocatalyst, actual analysis giving 19.9 wt.% Pt–Ru) was purchased from E-Tek. HP 20% Pt supported on carbon Vulcan XC-72 (Pt/C electrocatalyst, actual analysis giving 19.6 wt.% Pt on carbon) from E-Tek and a smooth Pt electrode were also required for comparative purposes. The ionomer was a 5% solution of Nafion perfluorinated ion-exchange resin in a mixture of aliphatic low molecular weight alcohols (isopropanol:*n*-propanol in weight ratio 55:45) and water (15–25 wt.% in the mixture), supplied by Aldrich. Glassy carbon disk (diameter 5 mm) and smooth Pt (diameter 3 mm) electrodes were provided by Metrohm. Analytical grade 96% H_2SO_4 from Merck and analytical grade 99.9% methanol from Panreac were used to prepare 0.50 M H_2SO_4 as the electrolyte for the CO stripping electrochemical experiments and the corresponding H_2SO_4–CH_3OH solutions for methanol oxidation measurements: 0.50 M H_2SO_4 + *X* M CH_3OH (*X* = 0.10, 0.25, 0.50, and 1.00) and 1.00 M CH_3OH + *Y* M H_2SO_4 (*Y* = 0.06, 0.21, 0.36, 0.64, and 0.92). All solutions were prepared with high-purity water obtained with a Millipore Milli-Q system (resistivity > 18 MΩ cm). H_2 and Ar gases were Linde 5.0 (purity ≥ 99.999%), while CO gas was Linde 3.0 (purity ≥ 99.9%).

2.2. Electrode preparation

Aqueous inks with electrocatalyst concentration of 5.0 mg ml^{-1} were prepared by sonicating for 45 min appropriate amounts of Pt–Ru/C or Pt/C electrocatalyst, Millipore Milli-Q water and the ionomer solution. The Nafion composition in the slurries was controlled in order to obtain in the dried inks a Nafion fraction in the range of 25–30 wt.%, which was determined in previous works [35,36] as the optimum ink composition that exposes the highest electroactive surface area, similar to the best performance composition found for DMFC tests in other papers [37–39]. According to the thin-layer method [2], stirred volumes of each ink around 7.0–10.0 μl were deposited by means of a digital micropipette (Labopette Variabel from Hirschmann or Witopet from Witeg) on the surface of the GC disk electrode, carefully weighting the deposited volumes with an AG 245 Mettler-Toledo analytical balance (accuracy of ±0.01 mg). The recently prepared electrodes were dried for 24 h in a clean dessicator at room temperature. Afterwards, the working electrode was ready to use in the Ecochemie Autolab RDE. The final Pt loads on the GC surface were 28 ± 2 μg cm^{-2}. Prior to the ink deposition, the GC tip was consecutively polished with aluminum oxide pastes of 0.3 and 0.05 μm (Buehler Micropolish II deagglomerated α-alumina and γ-alumina, respectively) on a Buehler PSA-backed White Felt polishing cloth until achieving a mirror finish, being rinsed with Millipore Milli-Q water in an ultrasonic bath between the polishing steps. The

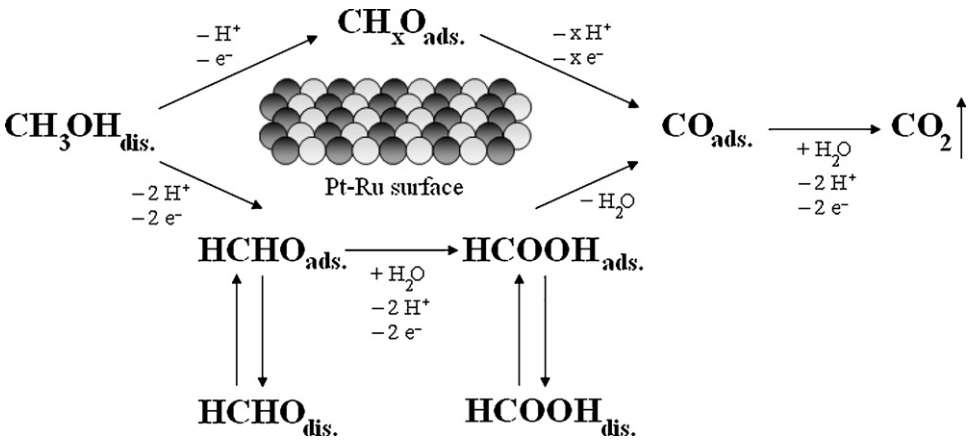

Fig. 1. Proposed methanol oxidation sequences on Pt-based electrocatalysts according to the literature evidences.

same treatment was made for the smooth Pt electrode. The GC coverage by the Pt–Ru/Nafion ink was determined from X-ray fluorescence (XRF) images (Fisher X-ray System XDAL spectrometer), which were analyzed using the Digital Micrograph 3.7.0 software, with values near 90% in most cases. The relative compositions of different regions of the deposited inks were also determined using the spectrometer facilities, thus allowing proving the ink homogeneity over the GC electrode.

2.3. Electrochemical measurements

All the electrochemical experiments were performed with a conventional thermostated double wall three-electrode glass cell from Metrohm of 200 ml capacity and an Ecochemie Autolab PGSTAT100 potentiostat–galvanostat with computerized control by an Autolab Nova 1.4 software. A Pt rod of 3.78 cm^2 apparent area was used as the auxiliary electrode and a double junction Ag|AgCl|KCl (saturated) electrode was employed as the reference electrode. All potentials given in this work are referred to the reversible hydrogen electrode (RHE) in the working electrolyte. The electrolyte was firstly deaerated by bubbling Ar for 30 min, and further 15 cyclic voltammograms at 100 mV s^{-1}, 15 more at 50 mV s^{-1} and 10 more at 20 mV s^{-1} between 0.02 and 1.00 V were consecutively performed under Ar atmosphere at 25.0 °C. They were practically quasi-stationary after the second scan, evidencing the stability and cleanness of the electrode. Cyclic voltammograms for CO stripping were conducted at 25.0 °C under Ar atmosphere at scan rates between 5 and 75 mV s^{-1}. The electrode was previously prepared by bubbling CO through the solution for at least 15 min and keeping the electrode potential at 0.01 V to assure the complete adsorption of CO on its surface. The CO remaining in the electrolyte was further removed by Ar bubbling for 30 min. The CO stripping charge obtained at the different scan rates were practically similar, indicating no electrocatalyst losses during the experiment.

The methanol oxidation reactions on the different electrocatalysts were studied in H_2SO_4–CH_3OH solutions. In all experiments, the electrolyte was previously deaerated by sparging Ar for 30 min and an Ar flow was kept over it during the potential cycling. A survey voltammogram was obtained by cyclic voltammetry between 0.20 and 1.00 V at 25.0 °C with a scan rate of 20 mV s^{-1} in 0.50 M H_2SO_4 + 1.00 M CH_3OH. Assays with different scan rates between 5 and 100 mV s^{-1} were also carried out at 25.0 °C in the same electrolyte by cyclic potential scan between 0.20 and 0.85 V. In the case of the RDE measurements, cyclic voltammograms between 0.20 and 0.85 V at 25.0 °C and scan rate of 20 mV s^{-1} were obtained at different rotation speeds (0, 1000, 2500 and 3600 rpm) in 0.50 M H_2SO_4 solutions with methanol concentrations between 0.10 and 1.00 M. Cyclic voltammograms between 0.20 and 0.65 V at 20 mV s^{-1} and 25.0 °C were recorded in 0.50 M H_2SO_4 + X M CH_3OH (X = 0.10–1.00), and in 1.00 M CH_3OH + Y M H_2SO_4 (Y = 0.06–0.92) for the determination of the methanol and proton reaction order, respectively. Methanol performance at different temperatures (25.0–45.0 °C) was monitored using cyclic voltammograms between 0.20 and 0.65 V in 0.50 M H_2SO_4 + 1.00 M CH_3OH electrolyte at 20 mV s^{-1}. For the determination of the adsorption isotherm parameters, the Pt–Ru/C-Nafion electrodes were immersed in 0.50 M H_2SO_4 + X M CH_3OH solutions (X = 0.10–1.00) at 25.0 °C for 30 min, then washed and transferred to a cell containing only 0.50 M H_2SO_4, where a cyclic voltammogram between 0.00 and 1.00 V at 25.0 °C was carried out to only oxidize the methanol adsorbed on the electrocatalyst surface. The methanol oxidation on Pt–Ru/C electrocatalyst in long-term experiments was analyzed in 0.50 M H_2SO_4 + 1.00 M CH_3OH by cyclic voltammetry between 0.00 and 1.00 V at 50 mV s^{-1} and 25.0 °C.

3. Results and discussion

3.1. CO oxidation on Pt–Ru/C electrocatalyst

The CO stripping voltammetry was applied to evaluate the electrocatalyst tolerance to poisoning by methanol derivatives, CO being the most representative product. Fig. 2 shows the cyclic

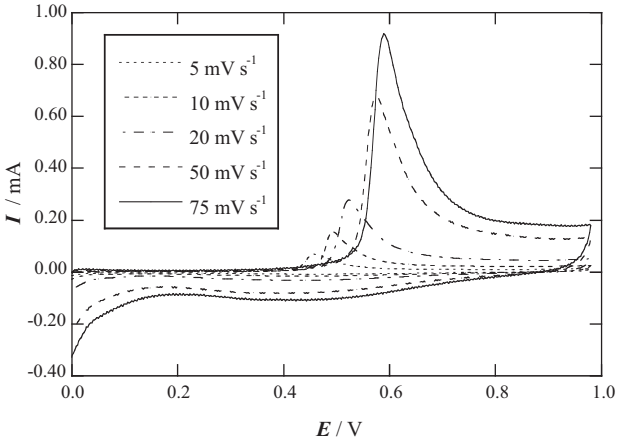

Fig. 2. Cyclic voltammograms for the oxidation of CO adsorbed on HP 20% 1:1 Pt–Ru/C Vulcan XC-72 electrocatalyst, in 0.50 M H_2SO_4 at scan rates between 5 and 75 mV s^{-1}, at 25.0 °C. CO was previously adsorbed at 0.01 V.

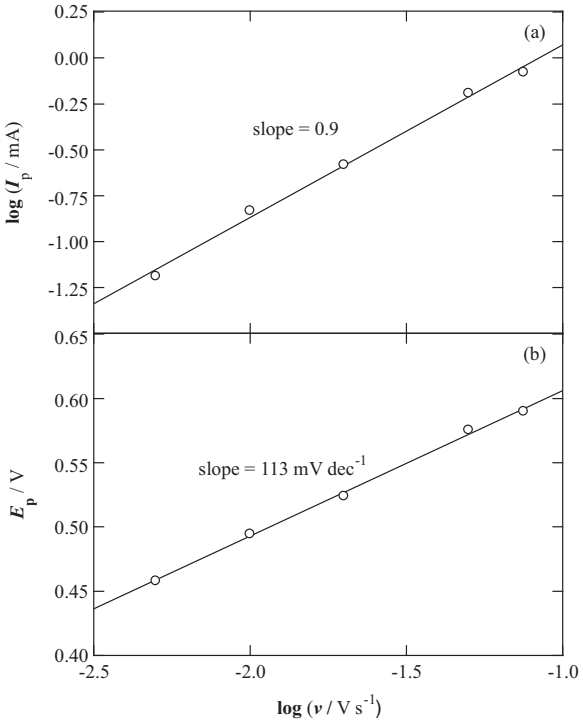

Fig. 3. (a) Log of peak current and (b) peak potential as function of the log of scan rate for the CO oxidation, corresponding to the cyclic voltammograms shown in Fig. 2.

voltammograms obtained in 0.50 M H_2SO_4 at different scan rates from 5 to 75 mV s^{-1}. An irreversible anodic peak related to the CO oxidation can be observed, attaining a peak potential of 0.46 and 0.59 V for 5 and 75 mV s^{-1}, respectively. Note that these potential values are much lower than the typical value of 0.80 V found for Pt [35], indicating the better tolerance of Pt–Ru/C in front of the CO poisoning.

The dependence of the peak current (I_p) and potential (E_p) with the scan rate (v) were then taken into account to analyse the CO oxidation reaction. Fig. 3a shows the good linear relation between $\log I_p$, and $\log v$, with a slope of 0.9, very close to the theoretical value of 1.0 for an adsorption-controlled reaction [40]. This confirms that the adsorbed CO molecule is oxidized on the electrocatalyst surface. Under these conditions, the peak potential (E_p) is related to v (V s^{-1}) by Eq. (6) [40]:

$$E_p = E^0 - \frac{2.3RT}{\alpha F}\log\left(\frac{RTk^0}{\alpha F v}\right) \quad (6)$$

where E^0 is the standard potential (V), R is the gas constant (8.314 J K^{-1} mol^{-1}), T is the temperature (298.1 K), α is the charge transfer coefficient, F is the Faraday constant (96497 C mol^{-1}) and k^0 is the rate constant for the electron transfer reaction (s^{-1}). Fig. 3b illustrates the excellent linear correlation found for the E_p–$\log v$ plot, with a slope of 113 mV dec^{-1}, very similar to the theoretical Tafel slope of 119 mV dec^{-1} predicted for a reaction with one-electron charge transfer as rate-determining step, the adsorbed intermediates following a Langmuir isotherm. From the experimental Tafel slope, an α value of 0.52 is then obtained. Taking into account the corresponding standard free energies of formation (ΔG_f^0) of the species involved in the reaction, E^0 = 0.104 V is found for CO oxidation. From this value and the Y-intercept of the plot in Fig. 3b, the calculated k^0 for the reaction (k_{CO}^0) is 7.5 × 10^{-5} s^{-1}. On the other hand, since one electron is transferred in CO oxidation, the surface concentration of adsorbed molecules (Γ_{CO}, in mol cm^{-2}) can be determined by Eq. (7) [40]:

$$I_p = \frac{\alpha F^2 A \Gamma_{CO}^v}{2.718RT} \quad (7)$$

where I_p is the peak current (mA) and A is the geometric electrode area (cm^2). Taking α = 0.52, Γ_{CO} = 1.6 × 10^{-7} mol cm^{-2} is obtained from data of Fig. 3a. The corresponding exchange current density, defined as $j_{0,CO} = nFk_{CO}^0\Gamma_{CO}$, was calculated, obtaining 2.3 × 10^{-6} A cm^{-2}. All the kinetic parameters for CO oxidation are summarized in Table 1.

Table 1
Kinetic parameters for CO oxidation on Pt–Ru/C electrocatalyst.

b_{CO}[a] (mV dec^{-1})	α_{CO}[b]	k_{CO}^0[c] (s^{-1})	$j_{0,CO}$[d] (A cm^{-2})
113	0.52	7.5 × 10^{-5}	2.3 × 10^{-6}

[a] Tafel slope for CO oxidation.
[b] Charge transfer coefficient for CO oxidation.
[c] Rate constant for the electron transfer reaction in CO oxidation.
[d] Exchange current density for CO oxidation.

3.2. Methanol oxidation on Pt–Ru/C electrocatalyst

Cyclic voltammetry in 0.50 M H_2SO_4 + 1.00 M CH_3OH was used in order to check the activity of the Pt–Ru/C electrocatalyst. For comparison purposes, the analogue electrocatalyst of pure Pt (Pt/C) was also tested. The corresponding cyclic voltammograms depicted in Fig. 4a confirm that both electrocatalysts present a good activity for methanol oxidation, which displays a well defined peak in the anodic scan. In the case of the Pt/C, the onset and the peak potential are located at 0.50 and 0.85 V, respectively. In contrast, the methanol oxidation on the Pt–Ru/C electrocatalyst starts at 0.30 V

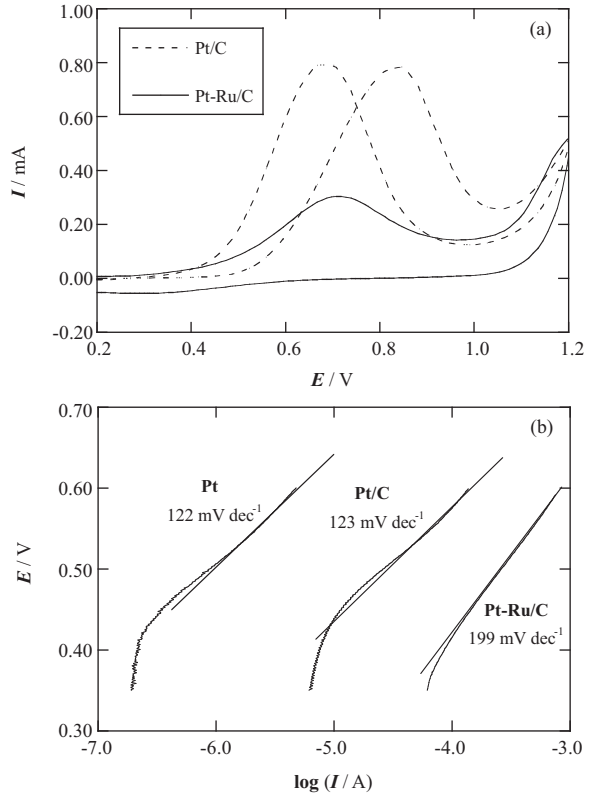

Fig. 4. (a) Cyclic voltammograms for methanol oxidation on HP 20% Pt supported on carbon Vulcan XC-72 and HP 20% 1:1 Pt–Ru/C Vulcan XC-72 in 0.50 M H_2SO_4 + 1.00 M CH_3OH solution at 20 mV s^{-1} and 25.0 °C. (b) Tafel plots for CH_3OH oxidation on different electrocatalysts under the same conditions.

Table 2
Kinetic parameters for CH_3OH oxidation on smooth Pt, Pt/C and Pt–Ru/C electrocatalysts.

Electrocatalyst	b_{MeOH}[a] (mV dec^{-1})	α_{MeOH}[b]	$j_{0,MeOH}$[c] (A cm^{-2})
Smooth Pt	122	0.48	3.2×10^{-9}
Pt/C	123	0.48	1.5×10^{-7}
Pt–Ru/C	199	0.30	7.4×10^{-6}

[a] Tafel slope for CH_3OH oxidation.
[b] Charge transfer coefficient for CH_3OH oxidation.
[c] Exchange current density for CH_3OH oxidation.

and achieves the peak potential at 0.70 V, so a reduction of about 0.20 V in the overpotential reaction is found when comparing with Pt/C. Note that this decrease is similar to the CO stripping peak potentials when the same electrocatalysts are compared, and one can suppose that the best performance for the methanol oxidation with the Pt–Ru alloy is due to the easier oxidation of CO that is generated as intermediate during the process. The higher peak current obtained for pure Pt (Fig. 4a) can be attributed to the existence of a greater concentration of actives sites for methanol adsorption in the nanoparticle surface, whereas a fraction of the nanoparticles can be covered by Ru or Ru oxides in the binary system leading to a smaller current. As previously discussed from XPS analyses [41], the studied Pt–Ru/C electrocatalyst also presents a kind of hydrous Ru oxide, typically called RuO_xH_y, which is considered very active for the methanol oxidation because of its proton- and electron-conductor, and water-dissociation properties [42–44], and then, the best performance achieved with the Pt–Ru/C electrocatalyst can also be explained considering the presence of this oxide.

Another interesting feature of the cyclic voltammogram of the Pt/C electrocatalyst is the presence of a prominent oxidation peak in the cathodic scan with a peak potential at about 0.70 V (Fig. 4a). A general explanation for the existence of this peak is the oxidation of the remaining carbonous species, with general structure CH_xO, generated during methanol oxidation reaction. Consequently, the ratio between the current in the forward and the reversal scan can be taken as an indication of the electrocatalyst efficiency. While this ratio is about the unity for pure Pt, it is much higher for Pt–Ru/C because the anodic peak in the reversal scan is practically undetectable, indicating that no carbonous species remain on its surface.

3.2.1. Tafel slope and exchange current density

The kinetic analysis for the methanol oxidation reaction on the Pt–Ru/C electrocatalyst was made considering the classical E vs. $\log I$ plot, presented in Fig. 4b. This figure also depicts the analogous Tafel plots obtained on smooth Pt and Pt/C. The electrocatalyst containing Ru has a better performance in the region under kinetic control (low overpotential) compared with the Pt/C, as stated above, whereas the oxidation current for the latter is much higher than that obtained for the smooth Pt because of its greater electroactive area. Excellent linear correlations are found between 0.45 and 0.60 V in all cases, and Table 2 collects the corresponding Tafel slopes thus obtained. Pure Pt and Pt/C present Tafel slopes very close to the theoretical value of 119 mV dec^{-1} ($\alpha = 0.50$), predicted for one-electron transfer reaction as rate-determining step and with the adsorbed intermediates following the Langmuir isotherm, as also found for the CO oxidation. However, in the case of Pt–Ru/C, this parameter offers a much higher value, 199 mV dec^{-1} ($\alpha = 0.30$), which can be accounted for by the different nature of the electrocatalyst surface, with the presence of Ru and Ru oxides and different adsorbed species. In the literature, the Tafel slope for methanol oxidation on Pt–Ru alloys varies from 60 mV dec^{-1}, using Pt single crystals covered by spontaneously deposited Ru at room temperature [29], to 180 mV dec^{-1} at 60 °C with bulk Pt–Ru alloy [9], obviously indicating that this parameter is strongly dependent on the catalyst morphology and the experimental conditions. The

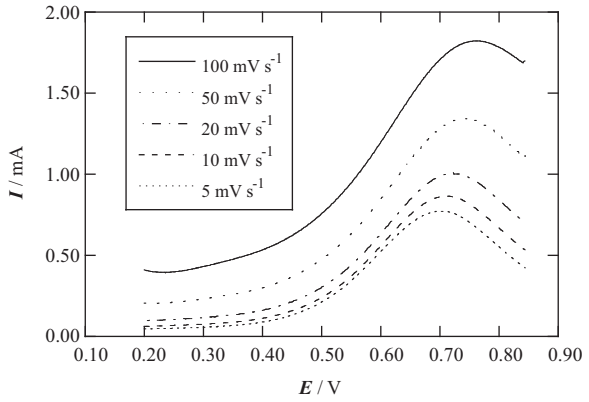

Fig. 5. Anodic sweep voltammograms for methanol oxidation on HP 20% 1:1 Pt–Ru/C Vulcan XC-72 in 0.50 M H_2SO_4 + 1.00 M CH_3OH at scan rates between 5 and 100 mV s^{-1}, and 25.0 °C.

exchange currents ($I_{0,MeOH}$) for methanol oxidation were then calculated by extrapolating the Tafel plots of Fig. 4b to the standard potential of the reaction (0.046 V), according to the Butler–Volmer approach, and its normalization by the geometrical electrode area yielded the corresponding exchange current densities ($j_{0,MeOH}$). These data are given in Table 2, where an increase in $j_{0,MeOH}$ in the order smooth Pt < Pt/C < Pt–Ru/C can be observed.

3.2.2. Effect of the scan rate in cyclic voltammetry

Fig. 5 shows the anodic sweep of the cyclic voltammograms recorded for methanol oxidation on Pt–Ru/C in 0.50 M H_2SO_4 + 1.00 M CH_3OH at scan rates between 5 and 100 mV s^{-1}. The increase in peak current with the scan rate can be analyzed considering an adsorption or diffusion control of the process. While for an irreversible process controlled by adsorption, the E_p–ν and I_p–ν relationships are given by Eqs. (6) and (7), respectively, the analogous expressions for a diffusion control [40] are:

$$E_p = E^0 + \frac{RT}{\alpha F}\left(0.780 + 2.3\log\left(\frac{D_0^{1/2}}{k^0}\right) + 2.3\log\left(\frac{\alpha F \nu}{RT}\right)^{1/2}\right) \quad (8)$$

$$I_p = 2.99 \times 10^5 A \alpha^{1/2} C_0 D^{1/2} \nu^{1/2} \quad (9)$$

where C_0 is the concentration in the bulk solution of the electroactive species (methanol, in mol cm^{-3}) and D_0 is the corresponding diffusion coefficient in the working electrolyte (cm^2 s^{-1}). A slope of 1.0 or 0.5 is then expected for the $\log I_p$–$\log \nu$ plots under adsorption or diffusion control, respectively, but Fig. 6a shows a much lower value of 0.23. A possible explanation for this behaviour is the existence of a kinetic contribution to the reaction control, as expected if the charge transfer for the methanol oxidation on Pt–Ru/C is considerably slow in the studied potential range taking place a mixed (diffusion-kinetic or adsorption-kinetic) control. For this reason, the apparent Tafel slope of 45 mV dec^{-1} obtained for the linear E_p–$\log \nu$ plot shown in Fig. 6b cannot be used to calculate the kinetic parameters for the methanol oxidation.

3.2.3. Effect of the rotation speed in the RDE

To clarify the nature of the methanol oxidation reaction, RDE experiments with different methanol concentrations from 0.10 to 1.00 M in 0.50 M H_2SO_4 were carried out. As can be seen in Fig. 7, the limiting current (I_l) for the corresponding anodic wave is practically unaffected by the rotation speed of the electrode. This agrees with the general result obtained with Pt electrodes [10], where the formation of Pt oxides, which present a poor activity for the methanol oxidation reaction, takes place at a potential lower than that necessary for achieving the diffusion control, and therefore, no

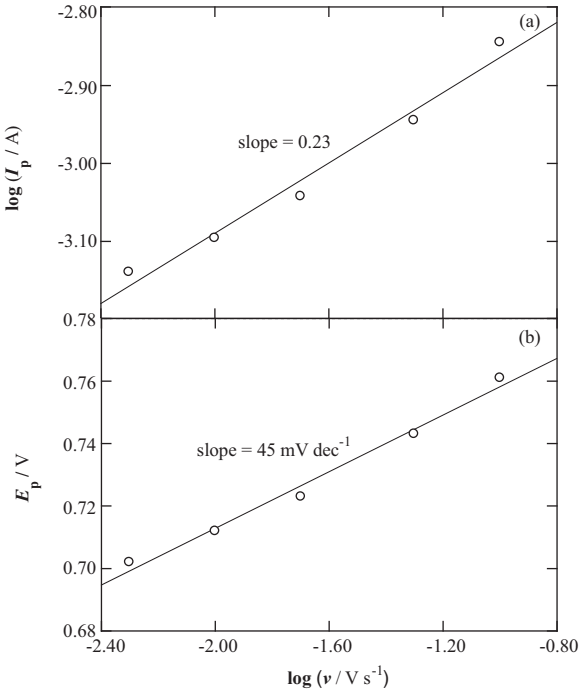

Fig. 6. (a) Log of peak current and (b) peak potential vs. log of scan rate for the methanol oxidation from the voltammograms presented in Fig. 5.

improvement of the current with the rotation speed is observed. In our case, the alcohol oxidation on Pt–Ru/C shows a similar performance. Previous work reported that the onset of the electrocatalyst surface oxidation in 0.50 M H_2SO_4 is around 0.80 V [41], close to the maximum of the limiting current, and for this reason, this generated oxide layer avoids that increasing convection leads to an increase of the anodic current. This blocking of the active surface can be the responsible of the kinetic reaction control contribution to the methanol oxidation discussed in relation to Fig. 6a. In contrast, the inset panel of Fig. 7 evidences a different trend using the smooth Pt electrode in RDE experiments. The I_l value is slightly suppressed by the increase of the electrolyte convection, which can be associated with the formation of a soluble intermediate that is weakly adsorbed on the electrocatalyst surface. This species could be HCOOH or HCHO, detected for the methanol oxidation on Pt electrodes [5]. When the electrode rotates, these intermediates can diffuse through the hydrodynamic

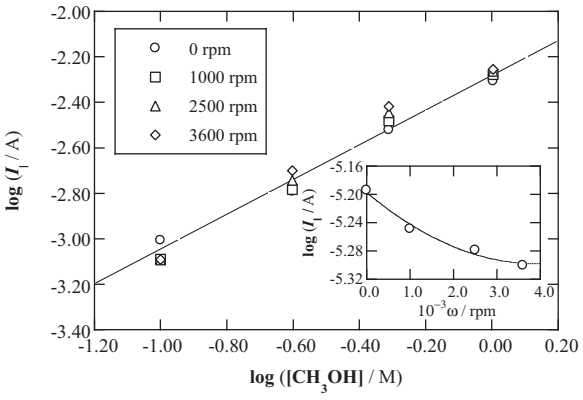

Fig. 7. Double logarithmic plot of current vs. methanol concentration for the alcohol oxidation on HP 20% 1:1 Pt–Ru/C Vulcan XC-72 by RDE at rotation speed up to 3600 rpm. The inset panel shows the logarithm of the limiting current in front of the rotation speed on smooth Pt. The RDE experiments were made in 0.50 M H_2SO_4 + 1.00 M CH_3OH at 20 mV s^{-1} and 25.0 °C.

layer to the bulk causing the observed decrease in current. However, the small reduction of I_l (about 20% at 3600 rpm) indicates that the soluble-intermediate mechanism is a minor path followed by the methanol oxidation at the Pt electrode. It seems thus reasonable to assume that the reaction mainly takes place through an adsorbed-intermediate mechanism, as described above, leading to the formation of CH_xO species and CO at least. Conversely, the fact that I_l is unaffected by the electrolyte convection when Pt–Ru/C is used, suggests that the soluble-intermediate mechanism is much less important. Other possibility is the restriction of the diffusion of generated soluble species because they remain in the vicinity of the electrocatalyst surface and are re-adsorbed by the carbonaceous support up to their further oxidation, thereby causing the independence of the current with the rotation speed. A similar behaviour has been reported by Gojkovic [10] for a carbon-supported Pt electrocatalyst.

3.2.4. Reaction order for the methanol and the proton

A cyclic voltammetric study was made for the oxidation of methanol in 0.50 M H_2SO_4 with 0.10–1.00 M of the reagent to calculate the reaction order for the alcohol (r) through the analysis of the anodic current in the region of low overpotential by Eq. (10) [45]:

$$r = \left(\frac{\partial \log I}{\partial \log[CH_3OH]} \right)_{T,E,\mathrm{pH}} \tag{10}$$

Fig. 8a shows the good straight lines obtained when plotting $\log I$ in front of $\log[CH_3OH]$ at low overpotential, with similar slopes close to 0.5. The positive sign of this slope indicates that the methanol oxidation is favoured by the reagent concentration, whereas its fractional value evidences that the rate-determining step involves adsorbed species generated during the reaction. Several authors have postulated that the initial step in methanol oxidation involves the adsorption of the alcohol molecule following a Temkin isotherm [12,16,25], which considers the interaction between the adsorbed species and that the adsorption energy decreases linearly with the coverage. This approach seems more accurate than the Langmuir isotherm, which does not consider the interactions between the numerous species produced during the reaction. For the methanol adsorption, the Temkin equation can be written as Eq. (11) [16]:

$$\theta = k + \frac{2.3}{f} \log[CH_3OH] \tag{11}$$

where θ represents the coverage of the methanol, k is a constant and f is the so-called inhomogeneity factor related to the distribution of adsorption sites with respect to the adsorption energy. Since the parameter θ cannot be directly obtained for different methanol contents, the amount of adsorbed methanol was determined in 0.50 M H_2SO_4 by the oxidation of the reagent previously adsorbed on the electrocatalyst surface by immersion of the electrode in different methanol solutions and using the charge Q involved in the oxidation process as parameter. This allows the definition of a reference concentration ($[CH_3OH]_{ref}$) related to its corresponding oxidation charge Q_{ref} and with a coverage θ_{ref}, verifying Eq. (11) as follows:

$$\theta_{ref} = k + \frac{2.3}{f} \log[CH_3OH]_{ref} \tag{12}$$

Subtracting Eq. (12) to Eq. (11), dividing by θ_{ref} and arranging the terms, one obtains:

$$\frac{\theta}{\theta_{ref}} = \frac{2.3}{f\theta_{ref}} \log\left(\frac{[CH_3OH]}{[CH_3OH]_{ref}} \right) + 1 \tag{13}$$

If the oxidation charge is proportional to the number of adsorbed methanol and intermediates molecules, one can consider that

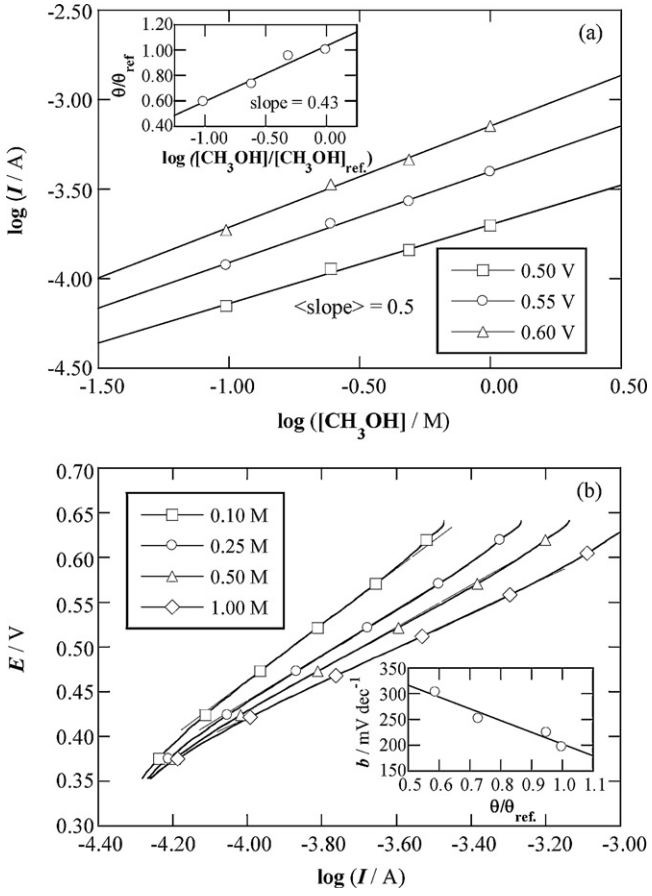

Fig. 8. (a) Double logarithmic plot of current against methanol concentration at different overpotentials for the alcohol oxidation on HP 20% 1:1 Pt–Ru/C Vulcan XC-72 electrocatalyst in 0.50 M H_2SO_4 at 20 mV s^{-1} and 25.0 °C. The inset panel gives the relative coverage (θ/θ_{ref}) vs. the relative concentration logarithm ($\log([CH_3OH]/[CH_3OH]_{ref})$). (b) Tafel plots in 0.50 M H_2SO_4 + (0.10–1.00 M) CH_3OH at 20 mV s^{-1} and 25.0 °C. The inset panel shows the Tafel slope against the relative coverage.

$Q/Q_{ref} = \theta/\theta_{ref}$ to evaluate the relative coverage of the electrocatalyst surface. Taking $[CH_3OH]_{ref}$ = 1.00 M as reference concentration, a good linear plot of Q/Q_{ref} vs. $\log([CH_3OH]/[CH_3OH]_{ref})$ with intercept close to the unity, in excellent agreement with Eq. (13), is obtained, as can be seen in the inset panel of Fig. 8a. From its slope of 0.43 and supposing an intermediate coverage of θ = 0.50, an inhomogeneity factor of 11 is found, very close to the usual f data of around 14–15 [16]. This good fitting of the experimental results to a Temkin isotherm confirms the validity of the employed method to analyse the adsorption of the methanol on the electrocatalyst surface.

The Tafel slopes were also evaluated when changing the methanol concentration between 0.10 and 1.00 M in 0.50 M H_2SO_4. Fig. 8b presents the corresponding Tafel diagrams, which exhibit well-defined linear regions in the low overpotential region with slopes changing from so high values as 293 mV dec^{-1} for 0.10 M CH_3OH to 199 mV dec^{-1} for 1.00 M CH_3OH. The trend of the Tafel slopes b cannot be justified using the classical Tafel law, given by Eq. (14), since the concentration does not explicitly appear as parameter:

$$b = \frac{2.3RT}{\alpha nF} \tag{14}$$

However, it may be associated to the variation of the electrocatalyst surface coverage (θ/θ_{ref}), as can be seen in the inset of Fig. 8b, indicating that the Tafel slope is strongly affected by the difference

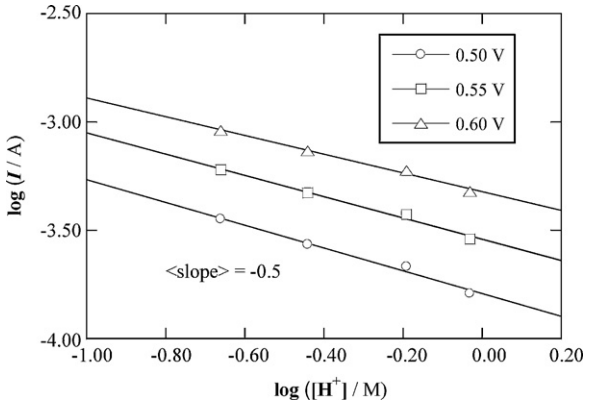

Fig. 9. Double logarithmic plot of current as a function of proton concentration for the methanol oxidation on HP 20% 1:1 Pt–Ru/C Vulcan XC-72 electrocatalyst in (0.06–0.92 M) H_2SO_4 + 1.00 M CH_3OH at 20 mV s^{-1} and 25.0 °C.

of the electrochemical environment in the outer layer of the Pt–Ru nanoparticles.

A cyclic voltammetric study was also carried out to know the reaction order for the proton (r') using 1.00 M CH_3OH in 0.06–0.92 M H_2SO_4. In this case, r' is defined by Eq. (15):

$$r' = \left(\frac{\partial \log I}{\partial \log[H^+]}\right)_{T,E,[CH_3OH]} \tag{15}$$

The plots of $\log I$ in front of $\log [H^+]$ at low overpotentials are depicted in Fig. 9. Good linear relationships with an average negative slope of $r' = -0.5$ can be observed, indicating that the methanol oxidation is inhibited by the increase in acidity of the media. The negative and fractional value of r' suggests that the proton appears as a product in the rate-determining step and in previous steps with intermediates adsorbed on the electrocatalyst surface. This supposition agrees with the methanol oxidation pathway following adsorbed-intermediate species, where CH_xO species are generated with a decreasing number of protons as the reaction advances until giving CO, which oxidation is considered as the rate-determining step.

3.2.5. Effect of the temperature on the methanol oxidation

Methanol oxidation experiments on the Pt–Ru/C electrocatalyst were also performed at different temperatures between 25.0 and 45.0 °C employing 0.50 M H_2SO_4 + 1.00 M CH_3OH solution as working electrolyte. The corresponding cyclic voltammograms (not shown) displayed an increasing oxidation current with rising temperature, as expected if the process is thermally activated. According to the Arrhenius law, the current in the region of low overpotential is related to the temperature in the logarithmic form from Eq. (16):

$$\log I = \log A - \frac{E_a}{2.3R}\left(\frac{1}{T}\right) \tag{16}$$

where A is the pre-exponential constant and E_a is the activation energy of the reaction. Fig. 10a illustrates the good linear and parallel plots obtained by plotting $\log I$ in front of T^{-1} in the region of 0.45–0.60 V, where the reaction is under kinetic control. From the average slope of 3.0×10^3 K, E_a = 58 kJ mol^{-1} is obtained, which is similar to the usual data of around 36–86 kJ mol^{-1} reported for Pt-based electrocatalysts in acidic electrolyte [7]. The calculated E_a can be attributed to the rate-determining-step, which is supposed to be the reaction (3) of the poisoning of Pt active sites (Pt–CO) with the neighbour hydroxylated Ru atoms (Ru–OH). The dissociative adsorption of methanol is discarded as rate-determining step because it presupposes a reaction order of 1.0, very different from 0.5 experimentally found, as stated above. Note in addition

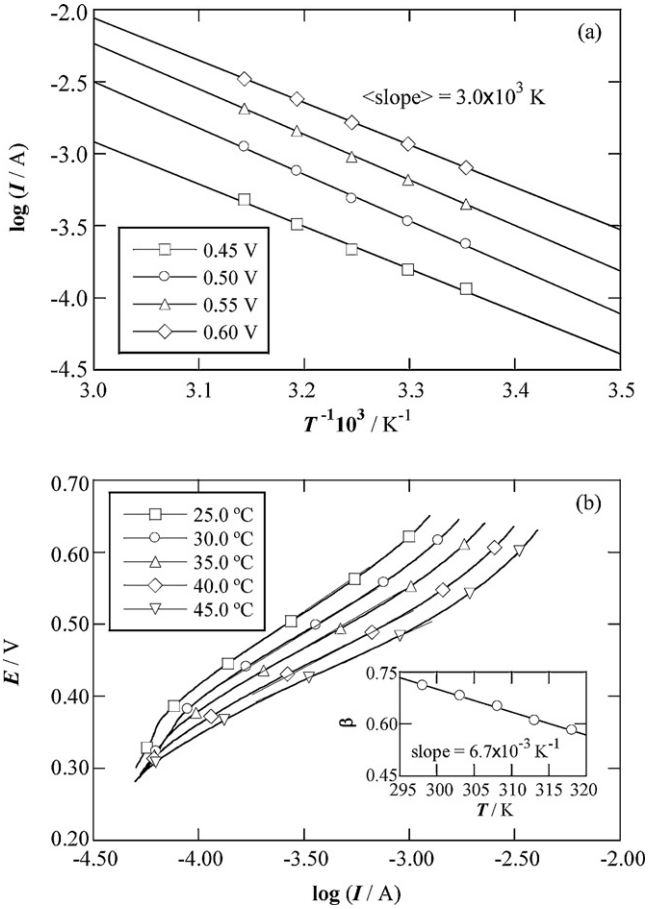

Fig. 10. (a) Arrhenius plots for the methanol oxidation on HP 20% 1:1 Pt–Ru/C Vulcan XC-72 electrocatalyst in the Tafel region using 0.50 M H_2SO_4 + 1.00 M CH_3OH at 20 mV s^{-1} and 25.0 °C. (b) Tafel plots under the same conditions at temperature between 25.0 and 45.0 °C. The inset panel depicts the change of the symmetry factor obtained from Tafel plots with the absolute temperature.

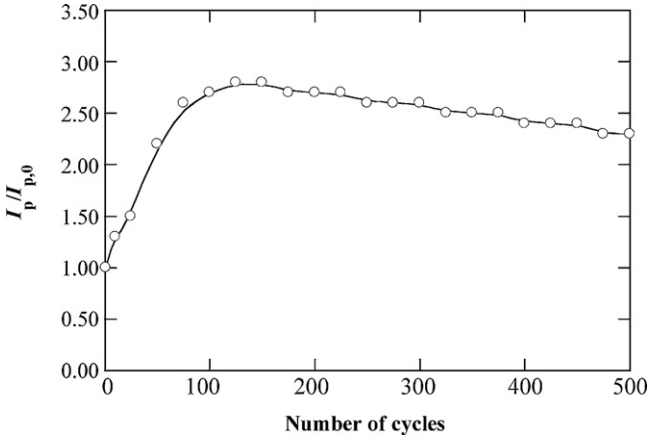

Fig. 11. Evolution of the normalized peak current with the number of cycles between 0.00 and 1.00 V determined for the anodic peak of methanol on HP 20% 1:1 Pt–Ru/C Vulcan XC-72 electrocatalyst in 0.50 M H_2SO_4 + 1.00 M CH_3OH at 50 mV s^{-1} and 25.0 °C.

that the calculated exchange current densities for carbon monoxide and methanol oxidation reactions present a similar value, being $\log j_0$ (A cm^{-2}) ≈ −5.5 for both processes, suggesting that the same rate-determining step is involved in both reactions.

Cyclic voltammograms at different temperatures were also employed to analyse the effect of the thermal parameter on the Tafel slopes for the methanol oxidation on Pt–Ru/C. Fig. 10b shows that the corresponding Tafel diagrams exhibit decreasing slopes as temperature increases, changing from 199 mV dec^{-1} at 25.0 °C to 150 mV dec^{-1} at 45.0 °C, which cannot be justified by the classical Tafel law (Eq. (14)). As a first approach, this anomalous phenomenon may be tentatively explained from the temperature-dependence of the apparent charge transfer coefficient [46–48]. For an anodic process with several steps and including adsorbed intermediates, the experimental α obtained from the Tafel slope is related to the symmetry factor (β) from Eq. (17) [48].

$$\alpha = \left(\frac{N-\gamma}{\nu}\right) - r\beta \tag{17}$$

where N is the number of electrons involved in the overall reaction, γ is the number of electrons transferred before the rate-determining step, r is the number of electrons passing in the rate-determining step and ν is the stoichiometric number, i.e., the number of times that the rate-determining step takes place for one act of the overall reaction. Considering that reaction (3) is the rate-determining step for the methanol oxidation and supposing that the adsorbed-intermediate pathway in the main mechanism route since the soluble-intermediate pathway is negligible (see Section 3.2.3), one can take $N = 6$, $\gamma = 5$, $r = 1$ and $\nu = 1$ in Eq. (17) to obtain $\alpha = 1 - \beta$, which allows calculating the symmetry factor value. The inset panel of Fig. 10b shows the linear plot found between β and T. Conway et al. [46] discussed a similar behaviour for the hydrogen and oxygen evolution considering that β corresponds to the addition of a temperature-independent enthalpy term (β_H) and a temperature-dependent entropic term ($\beta_S T$):

$$\beta = \beta_H + \beta_S T \tag{18}$$

By applying Eq. (18) to the linear fitting of β–T plot in the inset panel of Fig. 10b, one obtains $\beta_H = 2.8$ and $\beta_S = -6.7 \times 10^{-3}$ K^{-1}. The fact that β_H is higher than the unity indicates that the above model in not valid for the methanol oxidation.

Other authors pointed out that the change in the apparent α with temperature can be due to thermal secondary effects such as: (i) the change in the double layer structure that may alter the electrochemical environment of the system during the rate-determining step [47] and (ii) the change in the interaction of the adsorbed species, both intermediate species and anions, with the electrocatalyst surface that modifies the adsorption equilibrium and also causes a variation in the system vicinity [47].

3.3. Methanol oxidation on the Pt–Ru/C electrocatalyst in long-term experiments

A long-term cyclic voltammetric assay was carried out to test the performance of Pt–Ru/C electrocatalyst in 0.50 M H_2SO_4 + 1.00 M CH_3OH at 25.0 °C. A total of 500 potential scans between 0.00 and 1.00 V were done and the evolution of the peak current was monitored. Fig. 11 shows two different stages for the variation of the normalized peak current with the number of cycles applied. The initial stage corresponds to the first 100 cycles where the electrocatalyst is activated because the peak current increases 2.8 times with respect to that of the initial scan. For 100–150 cycles, a quasi-steady peak current can be observed, which afterwards undergoes a slow monotonic decrease up to a final value higher than twice the first peak current. The explanation of this trend is not trivial and can be related to the modification of the surface of the Pt–Ru nanoparticles. Several authors have reported that the current for the methanol oxidation is promoted when an anodic treatment is carried out, either by steady-state polarization at a selected potential higher than 0.9 V vs. RHE or by the performance of multiple scans up to 0.9–1.4 V as anodic limit [43,49–51]. The purpose of these treatments is the generation of hydrous ruthenium

oxide, RuO_xH_y, which is hypothesized to be more effective than Ru atoms because of their proton- and electron-conductor and water-dissociation electrocatalytic properties. Under our experimental conditions, the progressive oxidation of the electrocatalyst surface with RuO_xH_y production can explain the continuous improvement of the methanol oxidation during the first 100 cycles up to 1.00 V, attaining the maximum RuO_xH_y generation between 100 and 150 cycles. The further slight decrease in oxidation ability is a consequence of the reduction of the methanol concentration.

After the above assay, the used electrode was carefully washed, introduced in a fresh 0.50 M H_2SO_4 + 1.00 M CH_3OH solution and analyzed by cyclic voltammetry. The peak current recorded only decreased 0.98 times with respect to that of the fresh electrode, probably by the loss of electrocatalyst mass by the bubbling of CO_2 gas during the own long-term experiment. This allows concluding that the analyzed Pt–Ru/C electrocatalyst offers an excellent performance for the methanol oxidation in acidic media and a high stability. The effect of the oxidation of the alloy nanoparticle surface and its relationship with the improvement of the methanol oxidation will be deeper studied in future research.

4. Conclusions

The oxidation of carbon monoxide and methanol on carbon-supported Pt–Ru nanoparticles has been tested for their use in PEFC anodes. CO oxidation on the binary electrocatalyst behaved as an irreversible adsorption-controlled process with the reaction between the adsorbed Pt–CO and Ru–OH species as the rate-determining step under Langmuir conditions.

In the case of the methanol oxidation, the Pt–Ru/C electrocatalyst showed a better performance than Pt-electrocatalysts, offering a lower overpotential for the reaction, a higher exchange current density and negligible remaining intermediate subproducts (CH_xO, CO). The dependence of the anodic peak current on the scan rate indicated that the alcohol oxidation on the Pt–Ru/C electrocatalyst takes place according to a mixed control with a kinetic contribution, attributed to the generation of non-active Pt oxides on the nanoparticle surface. RDE measurements showed the practical independence of the oxidation current with the rotation speed for the carbon-supported Pt–Ru system, in contrast with the decreasing trend found for the smooth Pt electrocatalyst evidencing the generation of partially soluble intermediates, probably HCHO or HCOOH, simultaneously to the adsorption-intermediate process. For the Pt–Ru/C electrocatalyst, this pathway is less favoured because the presence of the high porous carbon support restricts the diffusion of soluble intermediates enhancing its oxidation. This evidences the importance of the substrate for avoiding efficiency losses in DMFCs.

Also for Pt–Ru/C, the reaction order for the methanol and the proton are fractional values of 0.5 and −0.5, respectively. The methanol adsorption follows a Temkin isotherm, whereas the negative sign for the proton agrees with the adsorbed intermediates mechanism, being the oxidation of generated CO the rate-determining step. Besides, the Tafel slope was found methanol-coverage dependent, indicating the influence of the different electrochemical environment. Cyclic voltammograms at different temperatures allowed obtaining an activation energy of 58 kJ mol^{-1}, whereas Tafel slopes did not verify the classical Tafel equation for the temperature dependence. This phenomenon cannot be explained by the change of symmetry factor and can be rather related to changes of the double layer structure and modifications of the interaction of adsorbed species.

A long-term cyclic voltammetric assay for the methanol oxidation on the Pt–Ru/C electrocatalyst showed an initial activation stage explained by the continuous generation of RuO_xH_y at high potential that enhances the alcohol oxidation capability. The subsequent decrease of the peak current was attributed to the depletion of the methanol concentration in the electrolyte, indicating that the analyzed Pt–Ru/C electrocatalyst exhibits an excellent performance for its employment in DMFCs.

Acknowledgements

The authors thank the financial support given by the Spanish MEC (Ministerio de Educación y Ciencia) through the project NAN2004-09333-C05-03. The grant from the Fundació Pedro Pons (Universitat de Barcelona) and the FPU fellowship from Spanish MEC received by A. Velázquez to do this work are also acknowledged. This work is dedicated to the memory of Amado Velázquez Méndez.

References

[1] T. Iwasita, Handbook of Fuel Cells-Fundamentals, Technology and Applications: Methanol and CO Electrooxidation, John Wiley & Sons, New York, 2003, Chapter 41, p. 603.
[2] W. Vielstich, A. Lamm, H.A. Gasteiger, Handbook of Fuel Cells-Fundamentals, Technology and Applications: Rotating thin film method for supported catalysis, John Wiley & Sons, New York, 2003, Chapter 22 p. 316.
[3] S. Alayoglu, A.U. Nilekar, M. Mavrikakis, B. Eichhorn, Nat. Mater. 7 (2008) 333.
[4] A.S. Arico, P.L. Antonucci, E. Modica, V. Baglio, H. Kim, V. Antonucci, Electrochim. Acta 47 (2002) 3723.
[5] E.A. Batista, G.R.P. Malpass, A.J. Motheo, T. Iwasita, Electrochem. Commun. 5 (2003) 843.
[6] J.H. Choi, K.W. Park, I.S. Park, W.H. Nam, Y.E. Sung, Electrochim. Acta 50 (2004) 787.
[7] J.L. Cohen, D.J. Volpe, H.D. Abruña, Phys. Chem. Chem. Phys. 9 (2007) 49.
[8] A.C. Garcia, V.A. Paganin, E.A. Ticianelli, Electrochim. Acta 53 (2008) 4309.
[9] H.A. Gasteiger, N. Markovic, P.N. Ross Jr., E.J. Cairns, J. Electrochem. Soc. 141 (1994) 1795.
[10] S.L. Gojkovic, J. Electroanal. Chem. 573 (2004) 271.
[11] S.L. Gojkovic, T.R. Vidakovic, Electrochim. Acta 47 (2001) 633.
[12] S.L. Gojkovic, T.R. Vidakovic, D.R. Durovic, Electrochim. Acta 48 (2003) 3607.
[13] D.J. Guo, L. Zhao, X.P. Qiu, L.Q. Chen, W.T. Zhu, J. Power Sources 177 (2008) 334.
[14] T. Iwasita, H. Hoster, A. John-Anacker, W.F. Lin, W. Vielstich, Langmuir 16 (1999) 522.
[15] X.H. Jian, D.S. Tsai, W.H. Chung, Y.S. Huang, F.J. Liu, J. Mater. Chem. 19 (2009) 1601.
[16] O.A. Khazova, A.A. Mikhailova, A.M. Skundin, E.K. Tuseeva, A. Havránek, K. Wippermann, Fuel Cells (2002) 99.
[17] H.T. Kim, H.I. Joh, S.H. Moon, J. Power Sources 195 (2010) 1352.
[18] H. Li, G. Sun, L. Cao, L. Jiang, Q. Xin, Electrochim. Acta 52 (2007) 6622.
[19] Y. Liang, H. Zhang, H. Zhong, X. Zhu, Z. Tian, D. Xu, B. Yi, J. Catal. 238 (2006) 468.
[20] D.G. Liu, J.F. Lee, M.T. Tang, J. Mol. Catal. A Chem. 240 (2005) 197.
[21] W.H. Lizcano-Valbuena, V.A. Paganin, E.R. Gonzalez, Electrochim. Acta 47 (2002) 3715.
[22] A.E. Russell, S.C. Ball, S. Maniguet, D. Thompsett, J. Power Sources 171 (2007) 72.
[23] J.R.C. Salgado, J.J. Quintana, L. Calvillo, M.J. Lázaro, P.L. Cabot, I. Esparbé, E. Pastor, Phys. Chem. Chem. Phys. 10 (2008) 6796.
[24] T.J. Schmidt, M. Noeske, H.A. Gasteiger, R.J. Behm, Langmuir 13 (1997) 2591.
[25] T. Seiler, E.R. Savinova, K.A. Friedrich, U. Stimming, Electrochim. Acta 49 (2004) 3927.
[26] Z.G. Shao, F. Zhu, W.F. Lin, P.A. Christensen, H. Zhang, J. Power Sources 161 (2006) 813.
[27] Z.G. Shao, F. Zhu, W.F. Lin, P.A. Christensen, H. Zhang, Phys. Chem. Chem. Phys. 8 (2006) 2720.
[28] J.M. Sieben, M.M.E. Duarte, C.E. Mayer, J. Appl. Electrochem. 38 (2008) 483.
[29] G. Tremiliosi-Filho, H. Kim, W. Chrzanowski, A. Wieckowski, B. Grzybowska, P. Kulesza, J. Electroanal. Chem. 467 (1999) 143.
[30] T. Vidakovic, M. Christov, K. Sundmacher, J. Electroanal. Chem. 580 (2005) 105.
[31] J. Wu, F. Hu, X. Hu, Z. Wei, P.K. Shen, Electrochim. Acta 53 (2008) 8341.
[32] X.H. Xia, T. Iwasita, F. Ge, W. Vielstich, Electrochim. Acta 41 (1996) 711.
[33] F. Ye, S. Chen, X. Dong, W. Lin, J. Nat. Gas Chem. 16 (2007) 162.
[34] X. Zhang, K.Y. Chan, Chem. Mater. 15 (2003) 451.
[35] I. Esparbé, E. Brillas, F. Centellas, J.A. Garrido, R.M. Rodríguez, C. Arias, P.L. Cabot, J. Power Sources 190 (2009) 201.
[36] A. Velázquez, F. Centellas, J.A. Garrido, C. Arias, R.M. Rodríguez, E. Brillas, P.L. Cabot, J. Power Sources 195 (2010) 710.
[37] A.S. Arico, A.K. Shukla, K.M. El-Khatib, P. Creti, V. Antonucci, J. Appl. Electrochem. 29 (1999) 673.
[38] K.H. Kim, K.Y. Lee, H.J. Kim, E. Cho, S.Y. Lee, T.H. Lim, S.P. Yoon, I.C. Hwang, J.H. Jang, Int. J. Hydrogen Energy 35 (2010) 2119.
[39] B. Krishnamurthy, S. Deepalochani, K.S. Dhathathreyan, Fuel Cells 8 (2008) 404.

[40] A.J. Bard, L. Faulkner, Electrochemical Methods, Fundamentals and Applications, John Wiley & Sons, New York, 1981, Chapters 6 and 14, p. 236 and p. 594.
[41] A. Velázquez-Palenzuela, F. Centellas, J.A. Garrido, C. Arias, R.M. Rodríguez, E. Brillas, P.L. Cabot, J. Phys. Chem. C 114 (2010) 4399.
[42] J.L. Gómez de la Fuente, M.V.M. Huerta, S. Rojas, P.H. Fernández, P. Terreros, J.L.G. Fierro, M.A. Peña, Appl. Catal. B Environ. 88 (2009) 505.
[43] M.K. Jeon, P.J. McGinn, J. Power Sources 198 (2009) 427.
[44] D.R. Rolison, P.L. Hagans, K.E. Swider, J.W. Long, Langmuir 15 (1999) 774.
[45] J.O.M. Bockris, S.U.M. Khan, Surface Electrochemistry: A Molecular Level Approach, Plenum Press, New York, 2003, p. 227, 1673.
[46] B.E. Conway, D.F. Tessier, D.P. Wilkinson, J. Electrochem. Soc. 136 (1989) 2486.
[47] E. Gileadi, J. Electrochem. Soc. 134 (1987) 117.
[48] E. Gileadi, E.K. Eisner, Corros. Sci. 47 (2005) 3068.
[49] S.Y. Huang, C.T. Yeh, J. Power Sources 195 (2010) 2638.
[50] Q. Lu, B. Yang, L. Zhuang, J. Lu, J. Phys. Chem. B 109 (2005) 1715.
[51] F. Scheiba, M. Scholz, L. Cao, R. Schafranek, C. Roth, C. Cremers, X. Qiu, U. Stimming, K. Fuess, Fuel Cells 6 (2006) 439.